Desalination and Water Treatment
www.deswater.com
doi: 10.5004/dwt.2020.26464

208 (2020) 125–135
December

Dehydration of caprolactam–water mixtures by composite membranes with nano silica/polyacrylate active layer by emulsion polymerization

Wenhai Lin[a,*], Zhenhua Liu[a], Qin Li[b], Qian Rong[c], Huajun Zu[a], Minghui Sang[a]

[a]*Advanced Functional Coating Additives R&D Center, Hefei University, China, emails: linwenhai@whu.edu.cn (W.H. Lin), liuzh@hfuu.edu.cn (Z.H. Liu), zuhuajun@sina.com (H.J. Zu), sangmh0808@sina.com (M.H. Sang)*
[b]*China Energy Engineering Group Anhui Electric Power Design Institute Co., Ltd., China, email: liqin@ahedi.com.cn (Q. Li)*
[c]*School of Materials Science and Engineering, Sun Yat-Sen University, China, email: rongq@mail2.sysu.edu.cn (Q. Rong)*

Received 3 February 2020; Accepted 17 August 2020

ABSTRACT

A pervaporation separation active layer by emulsion polymerization was prepared by using acrylate monomer and nano silica sol solution. Porous polyacrylonitrile substrate was used to construct composite pervaporation membranes. We used CPL/water mixture system (caprolactam (CPL)) to analyze the pervaporation separation performance of composite membranes, and studied the morphology and properties of the membranes by scanning electron microscopy, Fourier transform infrared, thermogravimetric analysis, X-ray diffraction, and contact angle. Given the formation of composite structures, the thermal stability of the nano silica/polyacrylate composite membrane is enhanced. A pervaporation transport equation was introduced to the permeation flux of normalized emulsion polymerization composite membranes. This equation relates to water permeability, CPL permeability, and membrane selectivity to assess pervaporation performance and potential mechanisms. The results show that the maximum total permeate flux of the CPL/water system reaches 1,138 g/(m^{2}h) with a separation factor of 353, which was remarkable compared with previous research. Membrane materials obtained by emulsion polymerization can be introduced to the field of pervaporation, providing a novel way to obtain excellent pervaporation membrane materials.

Keywords: Nanosilica/polyacrylate; Composite membrane; ε-Caprolactam; Pervaporation; Dehydration

1. Introduction

Pervaporation membrane needs different characteristics for different mixture systems. In order to obtain the best separation effect, it is an efficient way to adjust the flexibility and the swelling degree of the separation membrane. The nano silica/polyacrylate composite material was obtained by emulsion polymerization, and the method of pouring into pervaporation membrane can meet these requirements at the same time [1]. According to the requirements of the application system, the monomer ratio of short branched methyl methacrylate (such as methyl methacrylate) and long branched acrylate (such as butyl acrylate) can be adjusted, and different flexible polyacrylate membrane can be obtained easily through emulsion polymerization [2].

In the emulsion polymerization of polyacrylate monomer, the addition of nano silica can achieve two improvements: initially, the nano silica/polyacrylate composite prepared by emulsion polymerization has excellent compatibility [3]. The composite emulsion has low viscosity and good membrane forming property. After membrane formation, nano silica can improve the mechanical strength

* Corresponding author.

1944-3994/1944-3986 © 2020 Desalination Publications. All rights reserved.

and durability of the membrane, making it have attractive chemical stability and thermal stability [4]. Secondly, due to the existence of silica and silanol type hydroxyl, the surface of nano silica is negatively charged, which makes its surface highly hydrophilic. By controlling the content of nano silica, the permeability and separation effect of the composite membrane can be easily adjusted, and the appropriate separation flux and separation factor can be obtained. In addition, emulsion polymerization generally takes water as solvent, and has the advantages of fast polymerization speed, low dispersion, environmental friendliness, easy to heat dissipation, safety, low price, and easy batch production. Therefore, nano silica/polyacrylate composite has potential pervaporation value. However, the material has never been used for pervaporation dehydration and purification of ε-caprolactam (CPL).

CPL ($C_6H_{11}NO$) is a monomer of nylon-6, an industrially important organic chemical material widely used in the production of polyamide fibers and engineering plastics. The most common industrial process for CPL production is the Beckman rearrangement of cyclohexanone oxime. The most important impurity to be removed in the CPL is water, which is typically removed by distillation. CPL is unstable at high temperatures, so several traditional separation techniques, such as ion-exchange beds, electrodeionization [5], and solvent extraction [6], have been suggested to address this problem [7]. Three-effect evaporation processes are commonly used to produce high quality caprolactam. Conventional processes have disadvantages such as low heat transfer coefficient, high medium pressure steam consumption, and steam condensation with high CPL levels. Therefore, we investigated whether dehydration purification can be conducted by pervaporation [8–11]. However, our former attempts using pure polymer membranes by blending–casting process did not immediately reach a high flux, limiting the value of application. Further studies are necessary to enhance the application of pervaporation on the dehydration of CPL. We used *in-situ* emulsion polymerization to obtain a nano silica/polyacrylate composite with desired qualities and cast this composite emulsion for a PV membrane active layer, and dehydrated the caprolactam-water mixture through the pervaporation process (illustrated in Fig. 1).

2. Experimental

2.1. Materials

The industrial grade CPL is provided by Baling Petrochemical Co., Ltd., (China Petroleum and Chemical Corporation). Methyl methacrylate (MMA) and *n*-butyl acrylate (BA, industrial grade) were distilled before use. Silica sol (15 nm diameter) was purchased from Hubei Wuhan University Silicone New Material Co., Ltd. Sodium dodecylbenzenesulfonate (SDS, analytical reagent grade) was purchased from Sinopharm Chemical Reagent Co., Ltd. Polyacrylonitrile porous ultrafiltration membrane (cut-off molecular weight 5–10 × 10^4) was supplied by Shanghai Materials Research Institute (China). An aqueous feed solution for pervaporation experiments was prepared using deionized water.

2.2. Preparation of emulsions

Polyacrylate/SiO_2 emulsions were prepared by *in-situ* polymerization (Table 1). We added SDS, distilled water, and

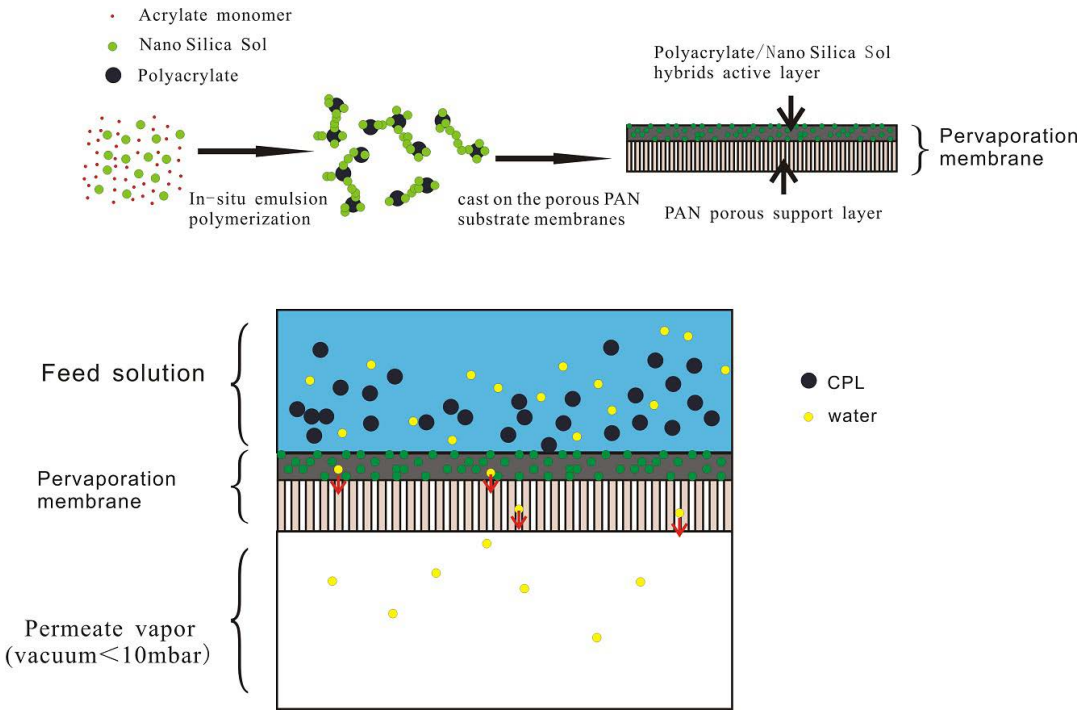

Fig. 1. Preparation and application of nano silica/polyacrylate PV membrane by emulsion method.

Table 1
Prescription of various silica sol/polyacrylate composite emulsions

Membrane	MMA (g)	BA (g)	SDS (g)	APS (g)	Silica sol (25 wt.% in the solution)	Water (g)
*M*0	20	20	1	0.32	0	200
*M*1	20	20	1	0.32	0.8	200
*M*2	20	20	1	0.32	3.2	200
*M*3	20	20	1	0.32	6.4	200
*M*4	20	20	1	0.32	16	200

nano silica sol to a 500 mL four-necked flask equipped with a stirrer, reflux condenser, and thermometer. The mixture was stirred for 2 h at a stirring rate of 400 rpm, and then MMA and BA were added. When the reaction temperature was heated to 75°C, amine persulfate dissolved in 8 g of distilled water was added to the mixture, which was then stirred at an agitation rate of 400 rpm for 3 h. After cooling the mixture to room temperature naturally, it was filtered to obtain the emulsion. The pure polyacrylate latex was prepared with the same procedure. It can be seen from Fig. 2a that the silica sol of the raw material is spherical particles with a particle size of 10–20 nm, and the latex particles obtained by emulsion polymerization are also spherical (Fig. 2b), and the particle size is smaller than 100 nm.

2.3. Preparation of nanosilica/polyacrylate composite membranes

The PAN ultrafiltration membrane was immersed in a 1.25 mol/L NaOH solution at 50°C for 60 min, and the membrane was repeatedly washed with deionized water to neutrality, and the membrane was immersed in a 1 mol/L HCl aqueous solution for 20 min, and washed with water to the neutral, obtained a hydrolyzed PAN microporous support membrane [12]. The porous PAN support membrane was fixed on a glass plate, and the prepared emulsion was brushed on the support membrane, and the water was slowly evaporated in a room temperature dust-free atmosphere until it was completely dried. Finally, the composite membrane was heat treated at 100°C in an air circulating oven. The pure polyacrylate is abbreviated as *M*0, and the polyacrylate hybrid membrane is abbreviated as *M*1–*M*4 according to different silica sol contents.

2.4. Swelling experiments

We performed an equilibrium swelling experiment using a *M*0–*M*4 membrane under the conditions of a 70 wt.% CPL solution at 30°C–60°C (same as the feed mixture). The dry membranes quality W_d was first weighed and immersed for 48 h at different temperatures in a sealed container to balance it. The membranes were taken out and the surface solution was wiped with a tissue paper and weighed as W_s. All experiments were performed at least three times and the results were averaged. The percentage of swelling (S) is calculated as:

$$S(\%) = \frac{(W_s - W_d)}{W_d} \times 100 \quad (1)$$

where W_d is the weight of the dry membrane and W_s is the weight of the swollen membrane.

2.5. Characterization

2.5.1. Fourier transform infrared spectroscopy

The emulsion nano silica/polyacrylate composite membranes were confirmed by Fourier transform infrared

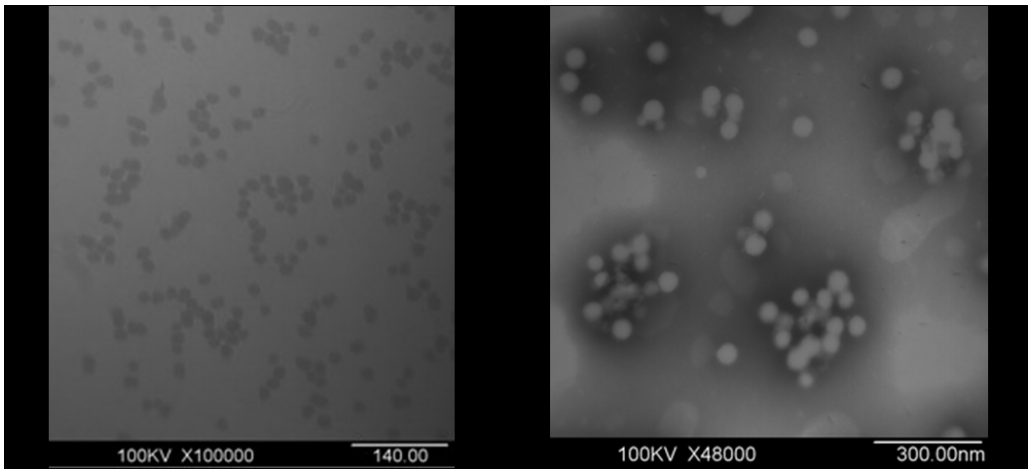

Fig. 2. (a) TEM spectra of silica sol and (b) nano silica/polyacrylate emulsions (10 wt.% nano silica).

(FT-IR) analysis. The FT-IR spectra of composite membranes *M*0–*M*4 were obtained using a Nicolet AVATAR 360 FT-IR spectrometer.

2.5.2. Scanning electron microscopy

The morphology of the composite membranes *M*0–*M*4 were examined by SEM (FEI Quanta 200, Holland). A layer of conductive gold is applied to all specimens.

2.5.3. X-ray diffraction analysis

The crystal structure of the composite membranes *M*0–*M*4 was analyzed by XRD measurement at a diffraction angle of 5° to 60° at a rate of 4°/min. The Shimadzu XRD-6000 (Japan) diffractometer is equipped with 40 kV and 30 mA graphite monochromatic Cu Kα radiation (λ = 1.54060 Å) at 40 kV and 30 mA.

2.5.4. Thermal analyses

Thermal gravimetric analysis was carried out by placing a 5–10 mg sample in an Al_2O_3 crucible, scanning from 20°C to 600°C at a heating rate of 10°C/min, and flowing at a flow rate of 50 mL/min in a nitrogen atmosphere. The instrument used is SETSYS 16 (France).

2.5.5. Contact angle analyses

The water contact angles on the surfaces of the composite membranes *M*0–*M*4 were measured at 25°C using a contact angle meter (Erma, model G–I). The contact angle θ was calculated with Eq. (2) [13]:

$$\theta = \cos^{-1}\left[\frac{\left(\cos\theta_a + \cos\theta_r\right)}{2}\right] \tag{2}$$

where θ_a is the advancing contact angle and θ_r is the receding contact angle.

2.5.6. Pervaporation experiments

The PV experiment of the membranes were carried out as follows: (1) The fixed feed mixture was 70 wt.% CPL. (2) The test temperature range is 27°C–47°C. At each temperature point tested, the membrane to be tested is equilibrated at the corresponding temperature for 1–2 h. (3) When the state is stable, at a fixed time interval, the permeate vapor is collected in a cold trap immersed in the liquid nitrogen jar on the downstream side.

On the basis of the PV data, the separation performance of the membrane was evaluated using PV flux (*J*) and separation factor (α). These two parameters are calculated using the following equations:

$$\alpha = \frac{\left(y_w / y_{\mathrm{CPL}}\right)}{\left(x_w / x_{\mathrm{CPL}}\right)} \tag{3}$$

$$J = \frac{W}{At} \tag{4}$$

In Eq. (3), x_{CPL} and x_w are the mole fractions of CPL and water in the feed, respectively; y_{CPL} and y_w are the mole fractions of permeate CPL and water, respectively. In Eq. (4), *W* (g) is the weight of the permeate, *A* (m^2) is the effective membrane area, and *t* (h) is the collection time.

3. Results and discussion

3.1. Membrane characterization

3.1.1. FT-IR analysis

The FT-IR spectra of pure polyacrylate, nano silica, and nano silica/polyacrylate composite membranes are illustrated in Fig. 3. The spectrum of pure polyacrylate shown in Fig. 3a shows that the characteristic bands at 2,887 cm^{-1} were attributed to C–H asymmetric stretching in the methylene of polyacrylate. The peaks at 1,452 and 1,391 cm^{-1} were due to the distortion vibration of CH_2. A strong and broad band at 1,727 cm^{-1} corresponded to the C=O stretching vibrations of carbonyl groups. In Fig. 3b, a peak at 1,118 cm^{-1} resulted from Si–O–Si asymmetric stretching vibration [14], and that at 475 cm^{-1} was attributed to Si–O–Si skeleton vibration and wagging vibration.

The spectra of nano silica-filled polyacrylate composite membranes (*M*1–*M*4) are displayed in Figs. 3c–3f. The characteristic absorption peak of the Si–O–Si skeleton at 475 cm^{-1} showed an increase in intensity compared with that of the unfilled *M*0 membrane in Figs. 3d–f. This finding indicated that the nano silica was enclosed in a polyacrylate matrix. Thus, nano silica particles were incorporated in the polyacrylate composite by *in-situ* emulsion polymerization.

3.1.2. SEM analysis

Fig. 4 shows the surface and cross-section morphologies of pure polyacrylate membranes. The outer surfaces of the membranes were dense and smooth. The cross-section pictures show that the pure polyacrylate active layer was tightly cast on the PAN porous support membrane. The thickness of the active layer was in the range of 2.5–3.5 μm, whereas the PAN porous support layer showed a thickness of 120 μm. Fig. 5 shows the surface and cross-section

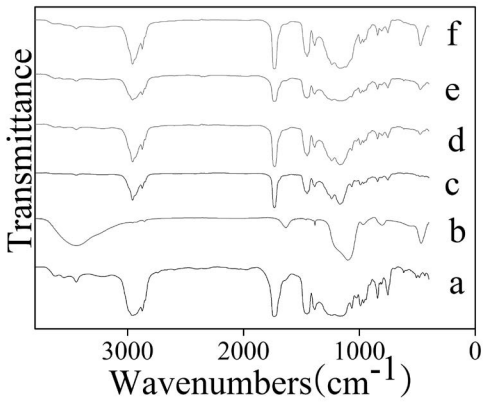

Fig. 3. FT-IR spectra of pure polyacrylate *M*0 (a) and original nano silica (b), nano silica/polyacrylate composite *M*1–*M*4 (c–f).

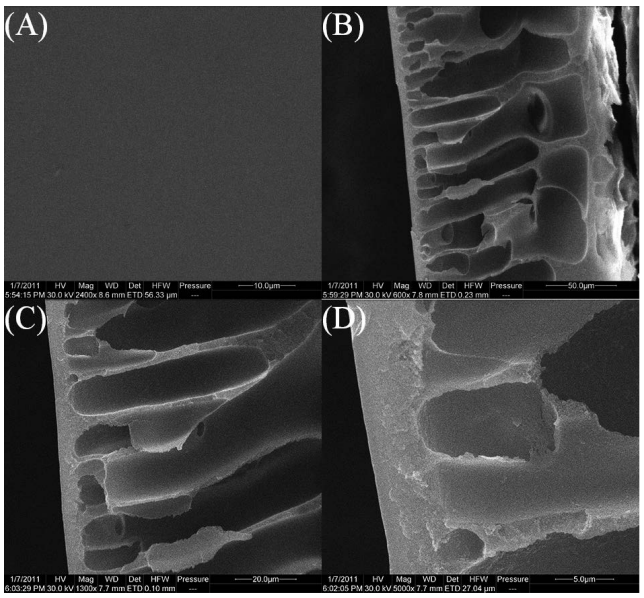

Fig. 4. External surface and cross-section morphologies of (A–D) pure polyacrylate membrane (*M*0).

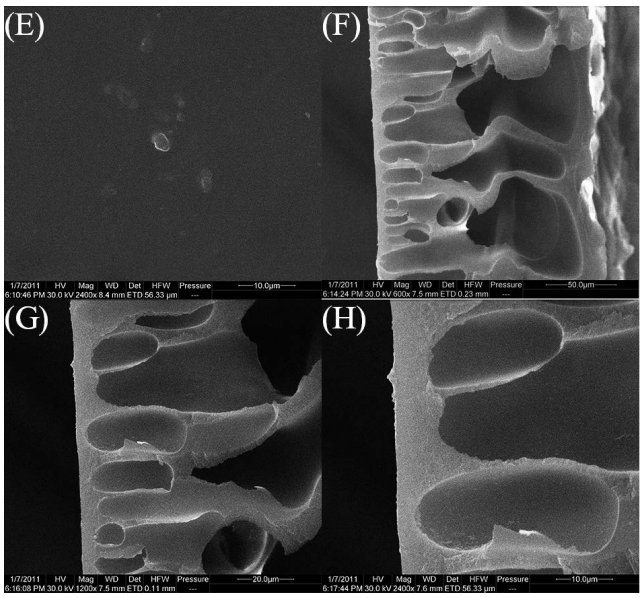

Fig. 5. (E–H) External surface and cross-section morphologies of nano silica/polyacrylate composite membrane (*M*2).

morphologies of nano silica/polyacrylate composite membranes. SiO_2 nanoparticles were dispersed on the active layer. The surfaces of the composite membranes with low SiO_2 nanoparticle content (2 wt.%) were rough but did not show serious aggregates of SiO_2 nanoparticles on the surfaces of the membranes. These results may cause a decrease in water contact angle, increase in permeation flux, and decrease in separation factor.

3.1.3. XRD analysis

XRD analyses were conducted on the flat-sheet films to investigate the influence of emulsion and incorporation of nano silica particles on the crystalline structure of the polyacrylate. As shown in Fig. 6, all samples show broad amorphous halo at $2\theta = 18°$, typical for lack of crystallinity. It is generally believed in the literature that adding a small amount of other particles to the ordered polymer will increase the amorphous degree of the composite, which is the same as our result [15,16]. The structure of the composite in the membrane is helpful for preferential penetration of water. This result is due to a decrease in crystallinity, which reduces the diffusion resistance and increases the free volume, thereby increasing the permeation flux of each component [17,18].

3.1.4. Thermal analysis

Fig. 7 compares the thermal stability of pure polyacrylate and nano silica/polyacrylate composite membranes using a decomposition curve. The thermal stability of the composite membrane is reduced by the order of *M*4 > *M*3 > *M*2 > *M*1 > *M*0. This phenomenon was attributed to the influence of nano silica dispersion in composite emulsion casting solution. Meneghetti and Qutubuddin [19] observed almost the same result when they prepared silica/polyacrylate nanocomposites by emulsion polymerization. Enhanced thermal resistance may be due to silica sol acting as an inorganic particle, forming a network structure when polymer was decomposed, trapping polymer chains in silica net, limiting its movement, and hindering further thermal decomposition. Moreover, nano silica was well dispersed in the polyacrylate matrix, acted as a gas barrier, prevented the diffusion of volatile gas from thermal decomposition process, and reduced the permeability of volatile gas [20].

3.2. Pervaporation characteristics

3.2.1. Swelling experiments

The study of the adsorption mechanism is important for controlling the pervaporation process of the membrane because it controls the chemical potential of the permeate molecules transported in the membrane. In pervaporation, the permeation flux and selectivity of the membrane depend on the degree of swelling of the active layer due to the interaction between the membrane and the CPL solution and the interaction between the CPL molecule and the water molecule. This section discusses the effects of sorption in pervaporation. To analyze the influence of nano silica on membrane swelling, we plotted the degree of swelling with different temperatures from 30°C to 60°C in a mass percent of CPL of 70 wt.% feed, as shown in Fig. 8.

The swelling degree of the membrane raised when the temperature increased but decreased as the nano silica level dropped. However, high nano silica contents in polyacrylate led to a low degree of swelling. XRD results confirmed that a high nanosilica concentration resulted in a compact amorphous region in the membranes (Fig. 6). Therefore, nano silica interfered with the array of polyacrylate molecular chain and increased the swelling degree. High levels of nanosilica resulted in a decrease in the degree of swelling because redundant nano silica could penetrate the membrane

and form a network structure; an increase in the network structure usually reduces the free volume of the membrane [11]. Thus, many nano silica composites result in low chain mobility and decreased degree of swelling.

3.2.2. Contact angle experiments

The contact angles are shown in Table 2. The contact angle reveals the surface properties. The SEM results revealed that the pure polyacrylate membranes demonstrated relatively smooth surfaces. Table 2 shows the change in wettability of the surface of the membranes after the addition of nano silica. The decrease in contact angle indicates an increase in surface hydrophilicity due to the interaction between the polyacrylate chain and the silanol of nano silica. Thus, water molecules easily dissolved on the surface of composite membranes. However, the change in contact angle is not linear with the nano silica content [21]. Few nano silica might react with the polyacrylate chain, resulting in a surface with increased hydrophilicity. Meanwhile, the composite membrane surface showed increased nano silica roughness and hydrophilicity and decreased contact angle. The SEM and contact angle results demonstrated good agreement. Our findings were validated by XRD experiments in Fig. 6 and swelling measurements in Fig. 8.

3.2.3. Influence of operating temperature

The effect of different feed temperatures on the pervaporation permeation flux and separation factor of the nano

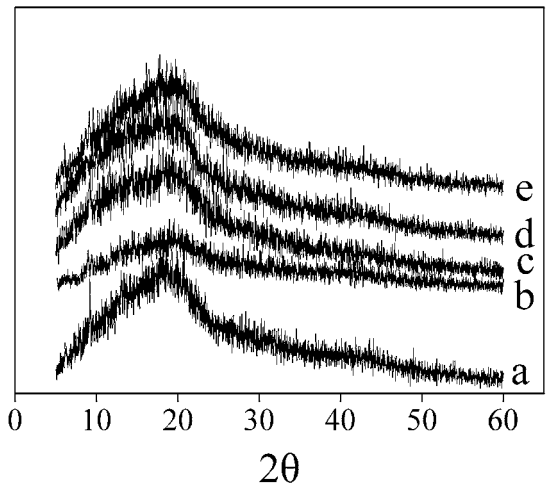

Fig. 6. XRD patterns of the pure polyacrylate membrane *M*0 (a) and nano silica/polyacrylate composite membranes *M*1–*M*4 (b–e).

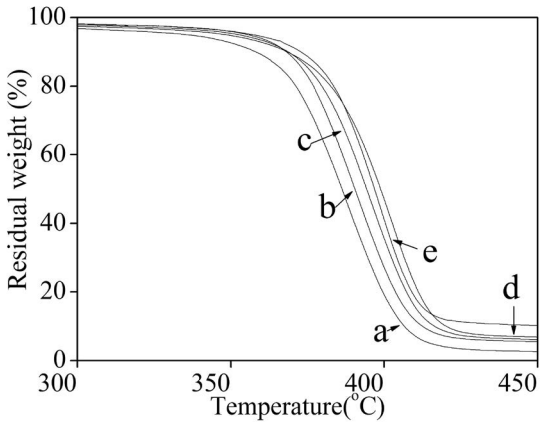

Fig. 7. TGA results of pure polyacrylate membrane *M*0 (a) and nano silica/polyacrylate composite membranes *M*1–*M*4 (b–e).

Table 2
Contact angles of water on pure polyacrylate membrane and nano silica/polyacrylate composite membranes

Abbreviations	Proportion in the membrane (wt.%)			Contact angle (°)	Photos
	MMA	BA	Nano silica		
*M*0	50	50	0	76 ± 1	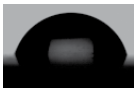
*M*1	49.75	49.75	2	71 ± 1	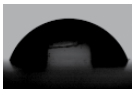
*M*2	49	49	2	71 ± 1	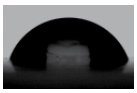
*M*3	48	48	4	70 ± 1	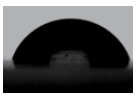
*M*4	45.5	45.5	9	70 ± 1	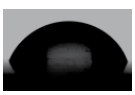

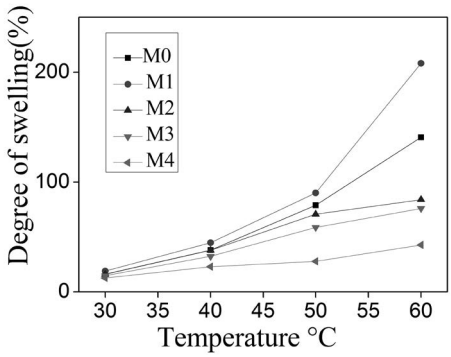

Fig. 8. Degree of swelling for 70 wt.% CPL solution in pure polyacrylate membrane and nano silica/polyacrylate composite membranes at different temperatures.

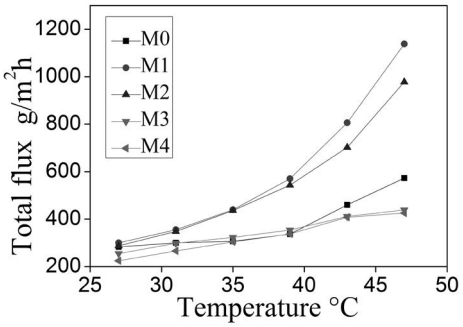

Fig. 9. Effect of nano silica content on pervaporation flux of composite membrane in 70 wt.% CPL aqueous solution at different temperatures.

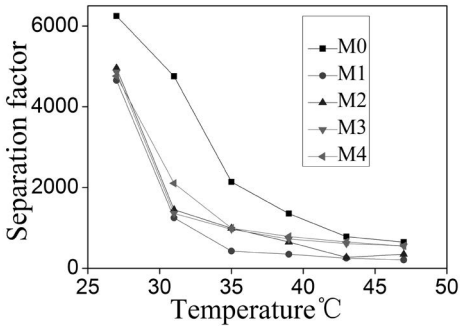

Fig. 10. Effect of nano silica content on separation factor of composite membrane in 70 wt.% CPL aqueous solution at different temperatures.

silica/polyacrylate composite membrane was investigated under 70 wt.% CPL feed conditions, as shown in Figs. 9 and 10. The nano silica/polyacrylate composite membranes demonstrated excellent thermal stability during pervaporation tests. Considering that CPL is a heat sensitive material, the operating temperature ranged from 27°C to 47°C. CPL aqueous solution became slightly light brown at 47°C, possibly due to a small amount of CPL in the feed liquid resulting from self-opening polymerization or oxidative degradation at high temperatures.

From 27°C to 47°C, the permeate flux increases, while the separation factor changes in the opposite direction. This is consistent with our previous work and trends reported in the literature [8,11]. The increase in feed temperature increases the solubility of the permeate in the membrane, the free volume in the composite membrane increases, and the movement of the permeate molecules accelerates, and the interaction between the permeate components becomes weak. The separation factor of all five selected membranes was opposite to the trend of temperature.

As the feed temperature increases, the diffusion rate of water and CPL molecules, the vibration frequency and amplitude of the polymer chain, and the free volume between the chains increase [22]. Separation factors decreased as the temperature increased, as shown in Fig. 10. The rise in temperature increased the swelling of the polyacrylate matrix, thereby facilitating the transport of CPL molecules and decreasing the separation factor. The correlation of the separation factor with temperature can be supported by the swelling experiment shown in Fig. 8. Each membrane underwent more than 10 h of PV experiments. After the test, the membrane can be removed intact, and has good elasticity and strength.

3.2.4. Activation energy analysis

The classical solution diffusion model expresses the permeate flux (J) as follows:

$$J = Q_{\text{water}}\left(p_{\text{water}}^{\text{feed}} - p_{\text{water}}^{\text{premeate}}\right) \tag{5}$$

$$J_{\text{CPL}} = Q_{\text{CPL}}\left(p_{\text{CPL}}^{\text{feed}} - p_{\text{CPL}}^{\text{premeate}}\right) \tag{6}$$

The permeability coefficient Q is defined as the difference between the permeation flux J divided by the partial vapor pressure P of each component, and the difference in vapor pressure is the driving force of pervaporation. The vapor pressure of the membrane feed side water and CPL can be calculated using Wilson's equation [11]. Based on the driving force in Eqs. (5) and (6), the permeation component transfer equation of the pervaporation process is defined according to the solution–diffusion model [23–25]:

$$p_{\text{water/CPL}}^{\text{feed}}\chi_i\gamma_i p_{i,\text{feed}}^{0} \tag{7}$$

$$p_{\text{water/CPL}}^{\text{permeate}} = y_i p_{\text{permeate}} \tag{8}$$

Two parameters in the driving force: the temperature sensitivity of the permeate activity coefficient (γ_i) and the saturated vapor pressure ($p_{i,\text{feed}}^{0}$) are different. When the temperature is raised, the activity coefficient (γ_i) of the permeate does not change much, but the saturated vapor pressure ($p_{i,\text{feed}}^{0}$) on the feed side increases rapidly, and the pressure is extremely low in the downstream under the action of vacuuming. Therefore, the saturated vapor pressure ($p_{i,\text{feed}}^{0}$) of the saturated vapor pressure on the feed side determines the driving force. The change in permeances is due to the combined effects of permeate flux and driving force. Membrane selectivity (β) is the ratio of the permeability of the two components [26].

$$\beta = \frac{Q_{water}}{Q_{CPL}} \tag{9}$$

The temperature dependence of the pervaporation flux and permeance can be expressed by Arrhenius equations.

The correlation between flux, permeance, and temperature is in accordance with the Arrhenius equation [23,28]:

$$J_i = J_0 \exp\left(\frac{-E_J}{RT}\right) \tag{10}$$

$$Q_i = Q_0 \exp\left(\frac{-E_Q}{RT}\right) \tag{11}$$

where J_0 and Q_0 are the pre-exponential factors; E_J and E_Q are the activation energy of the permeation flux and the membrane permeance, respectively; R is the gas constant (J mol^{-1} K^{-1}); and T is the absolute temperature (K).

The activation energies of permeates through the composite membrane can be estimated by measuring the slope of the lines in the diagrams. The difference between E_J and E_Q is the molar heat of vaporization ΔH_v.

Using the pervaporation flux and membrane permeance at different temperatures, combined with the absolute temperature T (K) and the gas constant R (J mol^{-1} K^{-1}), the permeation flux activation energy E_J and membrane permeance activation energy E_Q can be obtained by measuring the slope of the line in the graph according to the Arrhenius equation. The molar heat ΔH_v of pervaporation can also be obtained by calculating the difference between E_J and E_Q, which is expressed as [27]:

$$\Delta H_v = E_J - E_Q \tag{12}$$

Figs. 11 and 12 shows that the linear relationship between the logarithm of pervaporation flux and permeance and the reciprocal of temperature is good, which satisfies the Arrhenius equation. The activation energy values thus calculated are shown in Table 3. The total activation energy calculated from the total flux is 22.99 and 44.21 kJ/mol, respectively. Due to the influence of trace nano silica on the membrane structure, the latter is significantly higher than the former. Therefore, when the temperature is slightly increased in the composite membrane, the flux is significantly increased.

It can also be seen from Table 3 that the flux activation energy (E_J) of CPL is significantly higher than that of water, indicating that the transfer of CPL molecules on the membrane is more difficult than water. Compared with CPL, the activation energy of water is low, reflecting that nano silica/polyacrylate membrane is more suitable for dehydration of CPL/aqueous solution by pervaporation.

The physical structure and chemical composition of the membrane determine the permeance and selectivity, but the external conditions such as temperature have a great influence on the flux and separation factor [26]. It can be seen in Table 3 that the flux activation energy (E_J) is higher than the permeability coefficient activation energy (E_Q), which is consistent with the report in the literature: flux

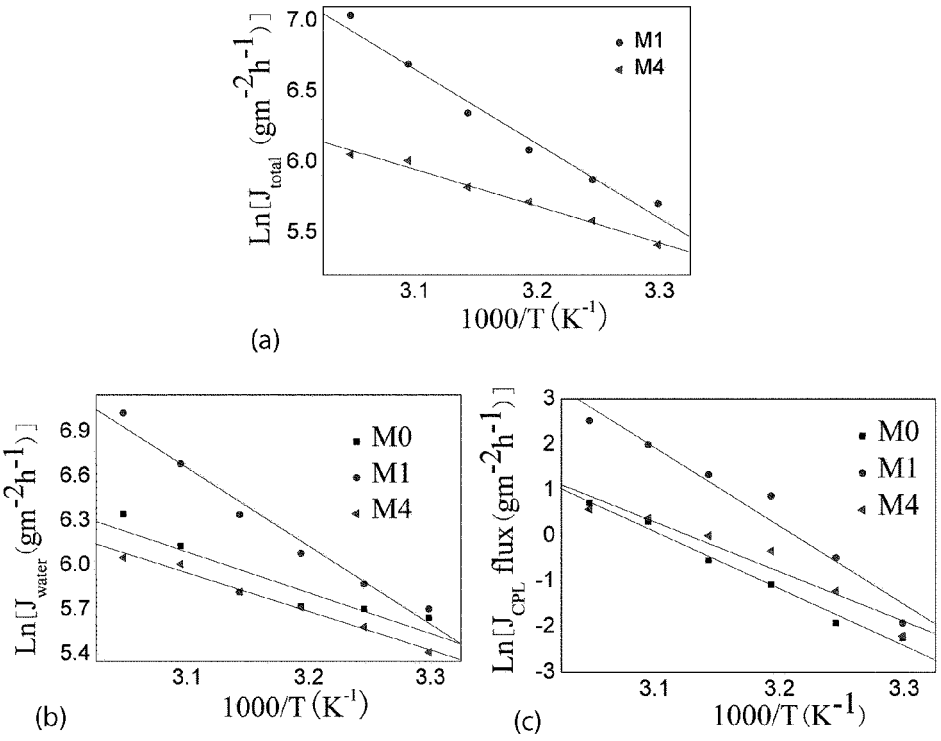

Fig. 11. Correlation between pervaporation total flux (a), water flux (b), CPL flux (c), and temperature for 70 wt.% CPL aqueous solution.

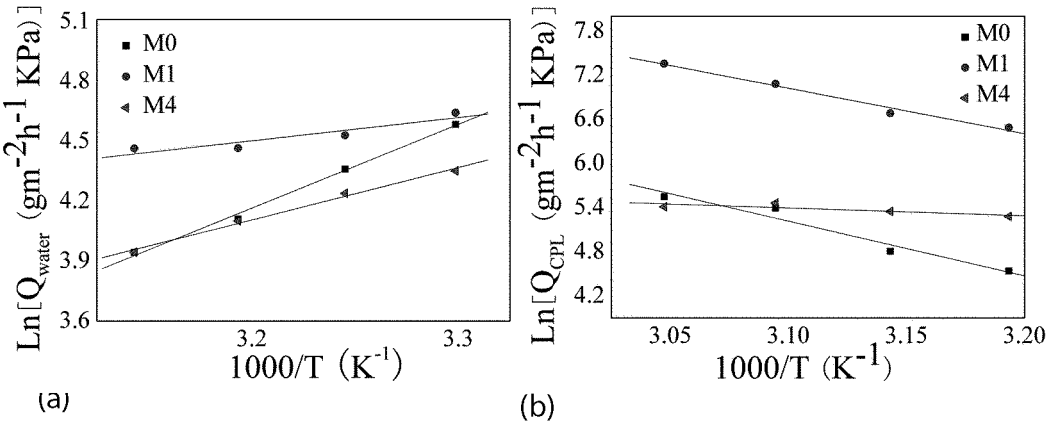

Fig. 12. Correlation between pervaporation water permeance (a), CPL permeance (b), and temperature for 70 wt.% CPL aqueous solution.

and separation factor are sensitive to feed temperature, while membrane permeance and selectivity are weak to temperature.

As shown in Table 3, when the downstream pressure ($p^{permeate}$) is very low compared to the upstream pressure (p^{feed}), the ΔH_v (Eq. (13)) value of water calculated by ($\ln(p^{feed} - p^{permeate})$ vs. $1/T$) is substantially the same, and the ΔH_v value of the CPL is also the same. The fluctuations caused by temperature effects are basically negligible. Therefore, the saturated vapor pressure (p^{feed}) of the feed solution determines ΔH_v, and it was near the phase transition enthalpy, as confirmed by our former work [11].

$$\left(p^{feed} - p^{permeate}\right) = A_0 \exp\left(\frac{-\Delta H_v}{RT}\right) \quad (13)$$

The comparison from Figs. 9–12 also shows that the effect of feed temperature on membrane permeances and selectivity is much weaker than on total flux and separation factor. This is because the membrane permeances and selectivity simply reflect the inherent separation performance of the membrane (Fig. 13), and the experimental operating conditions have little effect. The flux and separation factor parameters are not only dependent on the nature of the membrane, but also on the control of experimental operating conditions [28].

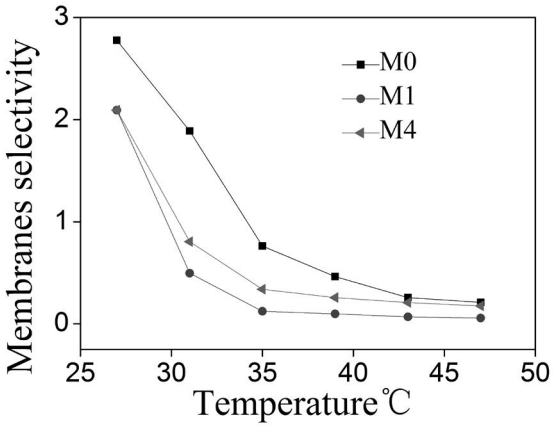

Fig. 13. Temperature dependence of membrane selectivity.

3.2.5. Effect of silica sol content

The effect of nano silica content on the pervaporation performance of the composite membrane is shown in Fig. 14. Surface modification is usually performed in optimal conditions [29]. In the present study, the surface of polyacrylate membranes treated with 0.5 wt.% nano silica showed the best flux performance. This result might

Table 3
Activation energy and molar heat ΔH_v of pervaporation data for nano silica/polyacrylate composite pervaporation membranes

Membrane	Activation energy (kJ/mol)					ΔH_v (kJ/mol)	
	Total	E_J		E_Q		Water	CPL
		Water	CPL	Water	CPL		
*M*0	22.99	22.88	106.71	–20.50	61.84	43.38	44.87
*M*1	44.21	43.85	96.19	0.47	51.31	43.38	44.88
*M*2	39.83	39.59	114.52	–3.79	69.65	43.38	44.87
*M*3	17.80	17.68	51.41	–25.70	6.53	43.38	44.88
*M*4	21.76	21.63	53.64	–21.74	8.77	43.37	44.87

Table 4
Comparison of separation performance of pervaporation membranes in literature

Membrane	Water content (wt.%)	T (K)	Flux (g/m^2/h)	Separation factor	Reference
PVA	30	328	900	1,500	11
PVA	40	318	650	1,600	11
PVA	40	313	450	2,000	11
PVA-CS	30	323	600	1,800	8
PVA-PAN	40	323	800	1,400	10
PVA-PAN	30	328	600	1,050	10
Composite *M*1	30	320	1,138	353	Present work
Composite *M*2	30	320	977	450	Present work

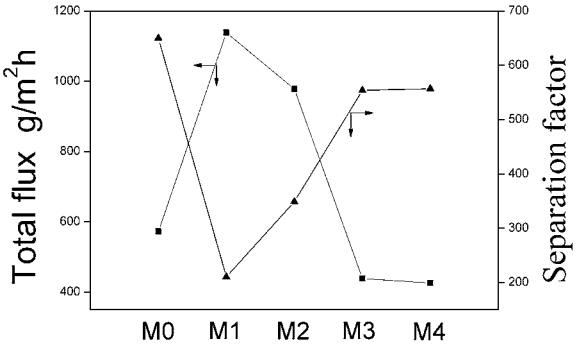

Fig. 14. Separation factor and total flux of pervaporation at 47°C using nano silica/polyacrylate composite membrane (70 wt.% CPL aqueous solution).

be attributed to the efficiency of silanol groups. However, water permselectivity decreased, which was in accordance with contact angle measurements. These effects contributed to the excellent hydrophilicity and plasticization effect of nano silica, and some formed intervals between polymer chains; however, additional nano silica may create a new regular structure, impeding the move of molecular materials, and negatively affecting the flux performance of composite membrane [29,30]. Our conclusions were validated by XRD experiments (Fig. 6) and swelling measurements (Fig. 8).

4. Conclusions

We prepared pure polyacrylate pervaporation membrane and nano silica/polyacrylate composite pervaporation membranes by *in-situ* emulsion polymerization. Characterization via FT-IR, TGA, and XRD revealed that nano silica modified the structure of polyacrylate. SEM demonstrated that the composite membranes' surface roughness and morphology differed from those of the pure polyacrylate membrane. Pervaporation results exhibited the high pervaporation flux performance of the nano silica/polyacrylate composite membranes compared with the pure polyacrylate pervaporation membrane and PVA-modified membranes (Table 4). The best performances of the composite membrane prepared with 0.5 wt.% nano silica at 47°C were obtained with the pervaporation flux J = 1,138 g/(m^2 h) and separation factor = 353.

All differences in the structural properties of composite membranes, surface morphology, and PV performance of membranes were attributed to interactions between nano silica and the polymer matrix. These interactions interfered with the array of polyacrylate molecular chain. The composites' structure was remarkable prior to water penetration through the membrane in pervaporation. The membrane material obtained by emulsion polymerization may be introduced to the pervaporation field, thereby providing an opportunity to find excellent pervaporation membrane materials for practical application.

Acknowledgments

This work was respectively supported by Anhui Provincial Natural Science Foundation (No. 1808085ME144), Anhui Province University Outstanding Youth Talent Support Program (No. gxyq2018070) and Research Fund of Hefei University (No. 19ZR08ZDA).

References

[1] M.M. Nazarabady, G. Farzi, Morphology control to design p(acrylic acid)/silica nano hybrids with controlled mechanical properties, Polymer, 143 (2018) 289–297.
[2] D.G. Gao, R. Chang, B. Lyu, J.Z. Ma, X.Y. Duan, Preparation of epoxy-acrylate copolymer/nano-silica via Pickering emulsion polymerization and its application as printing binder, Appl. Surf. Sci., 435 (2018) 195–202.
[3] A. Samanta, S. Takkar, R. Kulshreshtha, B. Nandan, R.K. Srivastava, Facile fabrication of composite electrospun nanofibrous matrices of poly(∈-caprolactone)-silica based pickering emulsion, Langmuir, 33 (2017) 8062–8069.
[4] C.L. Dai, H. Li, M.W. Zhao, Y.N. Wu, Q. You, Y.P. Sun, G. Zhao, K. Xu, Emulsion behavior control and stability study through decorating silica nano-particle with dimethyldodecylamine oxide at *n*-heptane/water interface, Chem. Eng. Sci., 179 (2018) 73–82.
[5] P. Yu, Z.H. Zhu, Y.B. Luo, Y.H. Hu, S.J. Lu, Purification of caprolactam by means of an electrodeionization technique, Desalination, 174 (2005) 231–235.
[6] M.L. van Delden, N.J.M. Kuipers, A.B. de Haan, Selection and evaluation of alternative solvents for caprolactam extraction, Sep. Purif. Technol., 51 (2006) 219–231.
[7] M. Poschmann, J. Ulrich, Franctional suspension crystallization with additional purification steps, J. Cryst. Growth, 167 (1996) 248–252.

[8] W.H. Lin, T.R. Zhu, Q. Li, S.P. Yi, Y. Li, Study of pervaporation for dehydration of caprolactam through PVA/nano silica composite membranes, Desalination, 285 (2012) 39–45.
[9] W.H. Lin, Q. Li, T.R. Zhu, New chitosan/Konjac glucomannan blending membrane for application in pervaporation dehydration of caprolactam solution, J. Ind. Eng. Chem., 18 (2012) 934–940.
[10] W.H. Lin, Q. Li, T.R. Zhu, Study of solvent casting/particulate leaching technique membranes in pervaporation for dehydration of caprolactam, J. Ind. Eng. Chem., 18 (2012) 941–947.
[11] L. Zhang, P. Yu, Y.B. Luo, Dehydration of caprolactam-water mixtures through cross-linked PVA composite pervaporation membranes, J. Membr. Sci., 306 (2007) 93–102.
[12] X.P. Wang, Modified alginate composite membranes for the dehydration of acetic acid, J. Membr. Sci., 170 (2000) 71–79.
[13] T. Uragami, K. Tsukamoto, K. Inui, T. Miyata, Pervaporation characteristics of a benzoylchiotsan membrane for benzene/cychlohexane mixtures, Macromol. Chem. Phys., 199 (1998) 49–54.
[14] M. Alagar, S.M.A. Majeed, A. Selvaganapathi, P. Gnanasundaram, Studies on thermal, thermal ageing and morphological characteristics of EPDM-g-VTES/LDPE, Eur. Polym. J., 42 (2006) 336–347.
[15] X. Wang, Y. Shen, X. Lai. Micromorphology and mechanism of polyurethane/polyacrylate membranes modified with epoxide group, Prog. Organ. Coat., 77 (2014) 268–276.
[16] J. Wang, Z. Han. The combustion behavior of polyacrylate ester/graphite oxide composites, Polym. Adv. Technol., 17 (2006) 335–340.
[17] X.H. Ma, Z.L. Xu, Y. Liu, D. Sun, Preparation and characterization of PFSA-PVA-SiO_2/PVA/PAN difunctional hollow fiber composite membranes, J. Membr. Sci., 360 (2010) 315–322.
[18] M.C. Burshe, S.B. Sawant, J.B. Joshi, V.G. Pangarkar, Sorption and permeation of binary water-alcohol systems through PVA membranes crosslinked with multifunctional crosslinking agents, Sep. Purif. Technol., 12 (1997) 145–156.
[19] P. Meneghetti, S. Qutubuddin, Synthesis of poly(methyl methacrylate)nanocomposites via emulsion polymerization using a zwitterionic surfactant, Langmuir, 20 (2004) 3424–3439.
[20] G.A. Wang, C.C. Wang, C.Y. Chen, Preparation and characterization of layered double hydroxides-PMMA nanocomposites by solution polymerization, J. Inorg. Organomet. Polym., 15 (2005) 239–251.
[21] X.J. Meng, Q.L. Liu, A.M. Zhu, Q.G. Zhang, Amino-functionalized poly(vinyl alcohol) membranes for enhanced water permselectivity, J. Membr. Sci., 360 (2010) 276–283.
[22] P. Sampraniboon, R. Jiraratananon, D. Uttapap, X. Feng, R.Y.M. Huang, Separation of aroma compounds from aqueous solutions by pervaporation using polyoctylmethylsiloxane (PDMS) membranes, J. Membr. Sci., 174 (2000) 55–65.
[23] J.G. Wijmans, R.W. Baker, A simple predictive treatment of the permeation process in pervaporation, J. Membr. Sci., 79 (1993) 101–113.
[24] J.G. Wijmans, Process performance=membrane properties + operating conditions, J. Membr. Sci., 220 (2003) 1–3.
[25] J.G. Wijmans, R.W. Baker, The solution-diffusion model: a review, J. Membr. Sci., 107 (1995) 1–21.
[26] Z. Huang, H.M. Guan, W.L. Tan, X.Y. Qiao, S. Kulprathipanja, Pervaporation study of aqueous ethanol solution through zeolite-incorporated multilayer poly(vinyl alcohol) membranes: effect of zeolites, J. Membr. Sci., 276 (2006) 260–271.
[27] X. Feng, R.Y.M. Huang, Pervaporation study of aqueous ethanol solution through zeolite-incorporated multilayer poly(vinyl alcohol) membranes: effect of zeolites, J. Membr. Sci., 118 (1996) 127–131.
[28] H.M. Guan, T.S. Chung, Z. Huang, M.L. Chng, S. Kulprathipanja, Poly(vinyl alcohol) multilayer mixed matrix membranes for the dehydration of ethanol-water mixture, J. Membr. Sci, 268 (2006) 113–122.
[29] M.X. Zou, S.J. Wang, Z.C. Zhang, X.W. Ge, Preparation and characterization of polysiloxane-poly (butylacrylate-styrene) composite latices and their membrane properties, Eur. Polym. J., 41 (2005) 2602–2613.
[30] F. Zhang, Y.P. Wang, C.P. Chai, Preparation of styrene-acrylic emulsion by using nano-SiO_2 as seeds, Polym. Int., 53 (2004) 1353–1359.